




# UVC radiation intensity dependence of pathogen decontamination rate: semiclassical theory and experiment

Nicolae A. Enaki<sup>1,a</sup> , Tatiana Paslari<sup>1</sup>, Sergiu Bazgan<sup>1</sup>, Elena Starodub<sup>1</sup>, Ion Munteanu<sup>1</sup>, Marina Turcan<sup>1</sup>, Vitalie Eremeev<sup>1,2</sup>, Aurelia Profir<sup>1,3</sup>, Ion N. Mihailescu<sup>4</sup>

<sup>1</sup> Quantum Optics and Kinetic Processes Lab of Institute of Applied Physics of Moldova, Chisinau, MD 2028, Republic of Moldova

<sup>2</sup> Instituto de Ciencias Básicas, Facultad de Ingeniería y Ciencias, Universidad Diego Portales, Av. Ejercito 441, Santiago, Chile

<sup>3</sup> Moldova State University Department of Computer Science, 60 Alexei Mateevici str., Chisinau MD-2009, Republic of Moldova

<sup>4</sup> National Institute for Lasers, Plasma and Radiation Physics, P.O. Box MG 36, 77125 Bucharest-Magurele, Romania

Received: 17 June 2022 / Accepted: 1 September 2022

© The Author(s), under exclusive licence to Società Italiana di Fisica and Springer-Verlag GmbH Germany, part of Springer Nature 2022

**Abstract** A semiclassical (light classical and molecule quantum) model describing the dependence of DNA/RNA dimerization rate as function of the ultraviolet C (UVC) radiation's intensity is proposed. Particularly, a nonlinear model is developed based on the Raman-like processes in quantum optics. The main result of the theory shows that the process of dimerization in the DNA/RNA depends strongly on the UVC light's intensity, thus proving a possible quantum microscopical mechanism of the interaction of UV light with the DNA. To corroborate the theoretical findings, we realize some experiments, by which want to investigate how the inactivation rate of the yeast colonies depends on the intensity of the UVC irradiation. The experimental results evidence a nonlinear decreasing of the residual yeast colonies as a function of the intensity in the irradiation process. The possibilities to optimize the intensity of UVC radiation in the considered decontamination equipment by using metamaterials are studied. The application of such equipment in disinfection of fluids (air, water, droplets, etc.), as well for the SARS-CoV-2-infected aerosols, is discussed.

## 1 Introduction

Ultraviolet radiation has been used for decades to disinfect unoccupied medical and other facilities and reduce the spread of airborne infectious diseases. Then, it is not surprising that ultraviolet C (known as UVC, 200–280 nm) light has recently gained particular attention as a promising control measure to reduce the transmission of SARS-CoV-2, the virus that caused the COVID-19 pandemic. Several investigations have shown that UVC is very effective in inactivating SARS-CoV-2 [1–6]. Therefore, this type of radiation can be used as an efficient disinfectant, but needs to be handled correctly to avoid skin and eye damage [7].

The growing need for decontamination of fluids, especially translucent ones as liquids, including water, gas, aerosols, air droplets, etc., opens up opportunities for innovative research in this direction [8–13]. Application of UV radiation for decontamination of fluids and surfaces from viruses and bacteria requires an effective method of inactivation of microorganisms by radiation. Open surfaces of translucent fluids cannot give us the expected result in this area due to the reduced penetration depth of UVC radiation into the fluid. For example, in [9, 10], we have analyzed the total contact surface with the contaminated fluid, formed due to the quasiperiodic optical system that contains quartz metamaterials, such as close-packed optical fibers or microspheres connected to each other through an evanescent UVC field. In this situation, an additional decontamination volume is obtained, which is proportional to the contact surface multiplied by the depth of transmission of UVC radiation inside the fluid. We can repack these periodic optical structures [11–13] to obtain a good evanescent zone necessary for decontamination of gas or liquids, which will flow near the total contact surface. In this case, we must estimate the adherence of the liquid (or infected aerosols and airborne droplets) to this surface and the penetration distance of the evanescent field in the translucent liquid. Based on this effect, we have elaborated two types of equipments for the decontamination of infected liquids and gases, see [8, 9]. These experiments have conclusively demonstrated that both, quartz spheres and optical fiber metamaterials, can effectively annihilate Coliform (including *Escherichia coli*), or *Enterococcus* bacteria, as well as yeast and kombucha cultures as described in [8]. The investigation of UVC radiation intensity dependence of decontamination in such metamaterial structures remains an open problem, and this work proposes to find connections between microscopic theory and experimental results.

For example, the work [8] was focused on estimating the critical intensity of the UVC field for which DNA/RNA pyrimidine dimerization becomes significant. Motivated by this idea, here we develop the disinfection model proposed in [10], using the quantum-theoretical approach to pyrimidine dimerization in DNA. In the normal state of DNA, it is known that the guanine (G) is

<sup>a</sup> e-mail: [enakinicolae@yahoo.com](mailto:enakinicolae@yahoo.com) (corresponding author)

paired with cytosine (*C*) through three hydrogen bonds, and adenine (*A*) is paired with thymine (*T*) through two hydrogen bonds. In the present work, we discuss the possible modifications and formation of new covalent bonds within neighboring pyrimidine bases of the same DNA strand under the action of UVC radiation [14–16].

As a matter of fact, in the last two decades, the interest to apply the quantum mechanical approach to the biological systems was particularly accentuated and many investigations were developed in this area, e.g., some of these [17–30]. The concept of *quantum biology* emerges mainly from the fact that at biological molecular level, the laws of quantum mechanics dominate. However, it is still far from being clear where lies the border that marks the domain of classical and quantum biological laws. For example, there are ideas to consider genes as quantum systems and describe them by a wave function based on the fact that in hydrogen bonds protons are shared between purines and pyrimidines and, respectively, are in a quantum superposition [18, 30]. On the other hand, there is strong skepticism about the true “quantum effects” in biological systems, mainly because the latter are highly decoherent and far from thermal equilibrium, so any coherent or superposition state is quickly lost. But, there can be an optimistic horizon, at least conceptually, one can think that such situations can be fixed, for example, loss of coherence and entanglement in quantum computation are considered “errors” and fortunately these can sometimes be corrected, procedure known as quantum error correction.

Of course, to identify and test quantum features of biological processes it is necessary to apply adequate empirical verification of theoretical approaches and predictions. There is already significant progress in this direction; for example, experimental findings in [19] show relatively long-time electronic quantum coherence in a photosynthetic protein under low-temperature conditions, around 77K. Furthermore, a little later it was shown that quantum coherence in similar proteins can survive even at room temperature [20, 21]. Such experimental results are very promising and strengthen the theoretical views on quantum properties in biology. Our work is a step towards this strategy with the main objective of experimentally testing our theoretical approach, where UVC radiation interacts with quantized molecules in the DNA dimerization process and showing how the inactivation rate of pathogens depends on UVC intensity.

This work is organized as follows: In Sect. 2, we propose a semiclassical model of Raman-scattered UVC radiation in DNA structure. This conceptual model applied for DNA/RNA dimerization process shows how the pathogen inactivation rate depends on the intensity of applied UVC field. The possible correlation of this theoretical approach with the experimental results is investigated in Sect. 3, where some realized experiments of decontamination of fluids are described. Particularly, we study the inactivation of yeast colonies applying the UVC radiation. As a result, by increasing the intensity of the applied UVC radiation in the decontamination core of the equipment, filled with metamaterials, we look on the effect of intensity dependence of the inactivation rate. Finally, in Sect. 4, we discuss the main approaches and results, and in Sect. 5, respectively, the work is concluded.

## 2 Theory: DNA/RNA dimerization as function of the intensity of UVC radiation through raman process

For the description of the intensity dependence of the modification of DNA structure under the action of the UVC radiation in this Section, we propose the Born-Oppenheimer (BO) approximation [31] used in chemistry and microbiology. In this approach, the nuclei subsystem is characterized by the vectors  $\mathbf{R} = \{R_1, R_2 \dots R_n\}$  and it is considered a slow subsystem as compared to the electronic subsystem in molecule,  $\mathbf{r} = \{r_1, r_2 \dots r_n\}$ . Here,  $R_1, R_2 \dots R_n$  and  $r_1, r_2 \dots r_n$  are the generalized coordinates of nuclei and bond electrons in a molecule. In this approximation, the molecular wave function is represented by the product  $|\Psi^{(e)}(\mathbf{r}, \mathbf{R})\rangle \otimes |\chi(\mathbf{R})\rangle$ , where  $|\Psi^{(e)}(\mathbf{r}, \mathbf{R})\rangle$  and  $|\chi(\mathbf{R})\rangle$  are the wave functions of electronic and nuclei subsystems of the molecule, respectively. The modification of the DNA and RNA structures takes place under the action of UVC radiation, as it is represented schematically in Fig. 1. Considering the nuclei positions fixed for the electronic subsystem, the Schrödinger equation can be represented in the form

$$H^{(e)}(\mathbf{r}, \mathbf{R}_s) |\Psi^{(e)}(\mathbf{r}, \mathbf{R}_s)\rangle = E^{(e)}(\mathbf{R}_s) |\Psi^{(e)}(\mathbf{r}, \mathbf{R}_s)\rangle. \quad (1)$$

Obviously, the electronic energy eigenvalue  $E^{(e)}$  depends on the chosen nuclei positions,  $\mathbf{R}_s$ . Varying these positions in small steps and repeatedly solving the Schrödinger equation of the electronic subsystem, one obtains  $E^{(e)}$  as a function of  $\mathbf{R}_s$ . We start with DNA's dimer modification of the adjacent nucleotide bonds,  $A = T$ , under the action of the electromagnetic field. The interaction energy of molecular electric multipoles may be approximated with the work of the electrical field during the displacements of electron at distance  $r_j$ , i.e.,  $H_{Int} = -\sum eV(r_j)$ , with the electric potential  $V(r_j) = \int_0^{r_j} E dr$  and neglecting the magnetic part of the field [32].

For the construction of the probable molecular states before and after the action of UVC radiation, we propose to represent the covalent bonds of the two adjacent nucleobases in DNA [34–36]. For example, the notations  $\{1 = 2\}$  and  $\{3 = 4\}$  represent two double covalent bonds between two adenine and thymine nucleotides. In the formation of the covalent bonds, electron orbitals overlap in order to form molecular orbitals, which give us the simplest prototype of molecule with covalent bonds observed in the  $H_2$  molecule in the archetypal Lewis pair

$$|\Psi_{H_2}(\zeta, R)\rangle = [2(1 + S_{ab})]^{-1/2} (|\varphi_a(1)\rangle \otimes |\varphi_b(2)\rangle + |\varphi_b(1)\rangle \otimes |\varphi_a(2)\rangle), \quad (2)$$

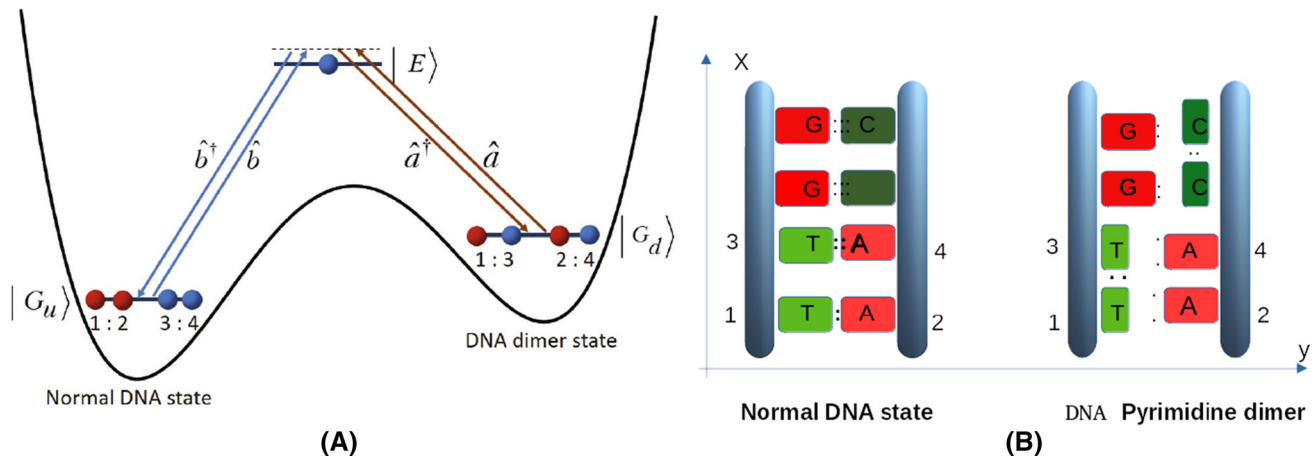


**Fig. 1** **A** Three-level description of the dimer bond generation by UVC radiation in DNA according to the literature. **B** Possible dimerization of thymine and cytosine in DNA under the UVC radiation. According to the literature [33], the ratio of  $T = T$  to  $C = C$  dimers is 10 : 1 or higher

where  $S_{ab} = [\int \varphi_a(r)\varphi_b(r)dr]^2$  is the overlap integral dependent on the orbital exponent,  $\zeta$ , and the internuclear separation,  $R$ . It is considered that a covalent bond is realized between two hydrogen-like atoms with two undistinguished electrons, 1 and 2, each of them may be localized in one of the states  $|\varphi_a(i)\rangle$  or  $|\varphi_b(i)\rangle$  near the nucleus  $a$  or  $b$ , with  $i = 1, 2$ .

Let us discuss the simple dimerization of DNA or RNA, in which thymine is replaced by uracil. The DNA strand breaks down to the dimerization state represented in Fig. 1(B) by the damage of two adjacent nucleobases,  $T = A$  and  $T = A$ , which pass into new bonds between thymine nucleotides,  $T = T$ , along  $x$ -direction of DNA strand. This process may be represented in the formalism of the three-level system of the collective electronic states. For example in double-stranded B-DNA, where the dimer entails two adjoining pyrimidine bases on the same DNA strand, only the *syn* isomers can be generated, whereas the *cis* isomer is preferred over the *trans* isomer to a great extent [33, 37].

Let us define the non-damaged ground state of the DNA strand by the wave function of two covalent bonds in the  $y$ -direction (see Fig. 1) as follows

$$\begin{aligned}
 |G_u\rangle &= |\Psi(\zeta, \mathbf{R}_{Iy})\rangle \otimes |\Psi(\zeta, \mathbf{R}_{Jy})\rangle, \\
 \text{where } |\Psi(\zeta, \mathbf{R}_{Iy})\rangle &= [2(1 + S_{ab})]^{-1/2} (|\varphi_a(1)\rangle \otimes |\varphi_b(2)\rangle + |\varphi_b(1)\rangle \otimes |\varphi_a(2)\rangle), \\
 |\Psi(\zeta, \mathbf{R}_{Jy})\rangle &= [2(1 + S_{cd})]^{-1/2} (|\varphi_c(3)\rangle \otimes |\varphi_d(4)\rangle + |\varphi_d(3)\rangle \otimes |\varphi_c(4)\rangle),
 \end{aligned} \quad (3)$$

are the two overlap bond states of adjacent nucleotides of DNA strands,  $\mathbf{R}_{Iy}$  and  $\mathbf{R}_{Jy}$ , respectively, which are represented by  $A : T(1, 2)$  and  $A : T(3, 4)$  in the  $y$ -direction of Fig. 1. For simplicity, we have represented in Eq.(3) only one covalent bond between each pair of nucleotides, but the nature of this ground state must be such that the precise recognition between  $C$  and  $G$  via triple H-bond, and between  $T(U)$  and  $A$  via a double H-bond, can guarantee the preservation of the genetic information encoded in the DNA (RNA) molecule [38, 39].

After the UVC action, the DNA steps chain pass into new states, where according to Fig. 1, the damaged “steps” passed into the new covalent bond state along the  $x$ -direction as follows

$$\begin{aligned}
 |G_d\rangle &= |\Psi(\zeta, \mathbf{R}_{Ix})\rangle \otimes |\Psi(\zeta, \mathbf{R}_{Jx})\rangle, \\
 \text{where } |\Psi(\zeta, \mathbf{R}_{Ix})\rangle &= [2(1 + S_{ac})]^{-1/2} (|\varphi_a(1)\rangle \otimes |\varphi_c(3)\rangle + |\varphi_c(3)\rangle \otimes |\varphi_a(1)\rangle), \\
 |\Psi(\zeta, \mathbf{R}_{Jx})\rangle &= [2(1 + S_{bd})]^{-1/2} (|\varphi_b(2)\rangle \otimes |\varphi_d(4)\rangle + |\varphi_b(4)\rangle \otimes |\varphi_d(2)\rangle)
 \end{aligned} \quad (4)$$

are the pyrimidine dimer and purine uncoupled nucleobases formed after modifications of step bonds between the DNA strands. We mention here that the purines (adenine and guanine) may remain uncoupled in covalent bonds (see Fig. 1). These two states are constructed in the process of absorption and emission of the two UV photons from the applied flux of UVC radiation.

The excited state contains the  $p$ -type wave function in which one of each of the four covalent electrons from the bonds  $a$ ,  $b$ ,  $c$  and  $d$  may be excited to

$$|E\rangle = |\Psi^{ex}(\zeta, \mathbf{R}_{Ix}, \mathbf{R}_{Jy})\rangle \quad (5)$$

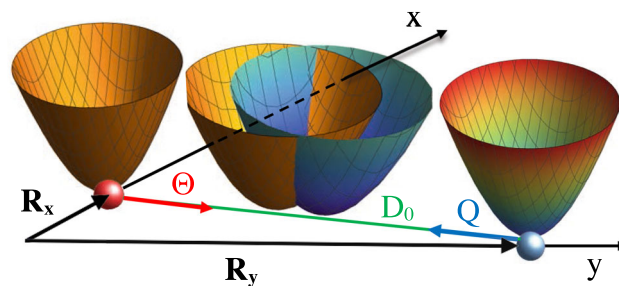


**Fig. 2** Illustrative sketch of the two minima of the same potential, one situated on the  $x$  axes corresponding to the pyrimidine state,  $T = T$ , and the second minimum is situated on the  $y$  axes corresponding to the normal state of DNA/RNA. The periodical excitation of the bond electrons by the radiation from normal state by the Raman-induced process moves nuclei positions of the pyrimidine dimer and normal states in opposite directions along the separation distance  $D_0$ , so that these two minima may overlap. This corresponds to the situation when the excited electrons may form the dimer (see overlap of the two paraboloids). When the radiation is turned off, these two minima of the potential energy return to their initial states on the  $x$  and  $y$  directions, but the large number of nucleotides remains in the dimer state

which is in an excited electron state  $|\varphi_a^{ex}(i)\rangle$  and may be in  $|2p\rangle$  or  $|2s\rangle$  hydrogen-like states as is described in the photosynthetic energy transfer [38–40, 44–46]. The electronic spectrum is protonated, thereby below we will show the possible excitation in such state as

$$|\Psi^{ex}(\zeta, \mathbf{R}_{Ix}, \mathbf{R}_{Iy})\rangle = N \sum_{i \neq l \neq n \neq m=1}^4 |\varphi_a^{ex}(i)\rangle \otimes |\varphi_b(l)\rangle \otimes |\varphi_c(n)\rangle \otimes |\varphi_d(m)\rangle, \quad (6)$$

where  $N$  is the normalization constant. Commonly, the energy  $E_{2s}$  of  $|2s\rangle$  state is lower than the energy  $E_{2p}$  of  $|2p\rangle$  state, and it is considered one or other excited state depending on the process that occurs. The optical transition between the same atomic states of hydrogen-like bonds with opposite parity,  $|E_{2s}\rangle = |\varphi_a^{1s}(i)\rangle$  and  $|E_{2p}\rangle = |\varphi_a^{2p}(i)\rangle$  with energies,  $E_{2s}$  and  $E_{2p}$ , respectively, may be larger than optical transition matrix element between the electron localization on different nuclei. Indeed, considering that in molecule, the overlapping between the states of different nuclei,  $|\varphi_a^{1s}(i)\rangle$  and  $|\varphi_b^{2p}(i)\rangle$ , may be less probable than the intrinsic transitions between the two ground states,  $|E_{2s}\rangle$ , and two excited states,  $|E_{2p}\rangle$ , of the same atom due to the small value of the ratio between the Bohr radius and mean distance between two atoms which participate in the covalent bond [34, 36].

We point out that due to delocalization of the excited electron, the dipole forbidden state nearby the nucleus may be excited by the shift of the states  $|1s\rangle_1$  to  $|2s\rangle_2$  of the nearby situated nuclei, labeled by 1 and 2. A brief review of such types of hybridization of the excited state, like  $\pi - \pi$ , stacking can be found in [38, 39] and a revised aspect of this concept is proposed in [40].

For simplicity, we neglect this type of transition  $|G_d\rangle \rightarrow |E_{2s}\rangle$ , so obtaining a three-level system with the electronic Hamiltonian,  $\hat{H}^{(e)} = \hat{H}_0^{(e)} + \hat{H}_{Int}^{(e)}$ , where

$$\hat{H}_0^{(e)} = -\hbar\omega_u|G_u\rangle\langle G_u| - \hbar\omega_d|G_d\rangle\langle G_d| + \hbar\omega_u^k \hat{b}_k^\dagger \hat{b}_k + \hbar\omega_d^k \hat{a}_k^\dagger \hat{a}_k, \quad (7)$$

$$\hat{H}_{Int}^{(e)} = -P_u^k g_k |E\rangle\langle G_u| \hat{b}_k - P_d^k g_k |E\rangle\langle G_d| \hat{a}_k + H.c., \quad (8)$$

are the free and interaction parts of the Hamiltonian, which describe the oscillation process between the three states of bimolecular formations as a normal, dimer and excited. Here  $P_u^k = |\langle G_u | \sum_j e_j(\mathbf{r}_j, k) | E \rangle|$  is the electronic polarization relative to the molecular transition  $|G_u\rangle \rightarrow |E\rangle$ ,  $P_d^k$  is a similar polarization relative to the dimer transition,  $|G_d\rangle \rightarrow |E\rangle$ , and  $k$  is polarization of the applied UVC radiation. In the following one defines  $\mathcal{E}_u(R_s) \equiv \hbar\omega_u$  and  $\mathcal{E}_d(R_s) \equiv \hbar\omega_d$  as the energies between the  $|E\rangle$  state and the two ground states,  $|G_u\rangle$  and  $|G_d\rangle$ , respectively. These energies are nearby the excitation quanta energies of the applied field,  $\delta_u = \omega_u - \omega_u^k$  and  $\delta_s = \omega_s - \omega_s^k$ . The creation (annihilation) operators,  $\hat{b}_k^\dagger, \hat{a}_k^\dagger$  ( $\hat{b}_k, \hat{a}_k$ ), are responsible for the excitation and de-excitation processes relatively to the two ground states described by the transitions  $|G_u\rangle \leftrightarrow |E\rangle$  and  $|G_d\rangle \leftrightarrow |E\rangle$ , respectively. As commonly, for the twice repeated index  $k$ , one considers the summation over the photon wave vectors of pump and Stokes fields.

In the following, let us consider the situation in which the excited state,  $|E\rangle$ , is off resonance with the external UVC field, thereby the transition between two ground states,  $|G_u\rangle$  and  $|G_d\rangle$ , takes place virtually through the polarization relative to the excited state. The procedure of elimination of electronic subsystem and its action on the energy renormalization of the position of the atomic potential and bounds between them is given in Appendix A.

According to the illustrations in Figs. 1 and 2, we may introduce the new generalized oscillation coordinates relative to the minimal energy of the normal and dimer states of the DNA section in the absence of external field. We point out that in Fig. 2 the right potential corresponds to the normal state of thymine and the left one corresponds to the dimer state. In the absence of the UVC radiation, these states are separated, i.e.,  $D_0 > |Q|$ , and according to this situation, the thymine nuclei rings are in one of the Fock states,  $|n\rangle_u$  or  $|n\rangle_d$ . The first eigenvector corresponds to the solution of the oscillator equation

$$(-\hbar^2 \Delta_Q / (2M_u) + M_u \Omega_u^2 Q^2 / 2) |n\rangle_u = \hbar \Omega_u (n + 0.5) |n\rangle_u$$

and the second corresponds to possible pyrimidine dimerization of DNA/RNA after the action of the electromagnetic field

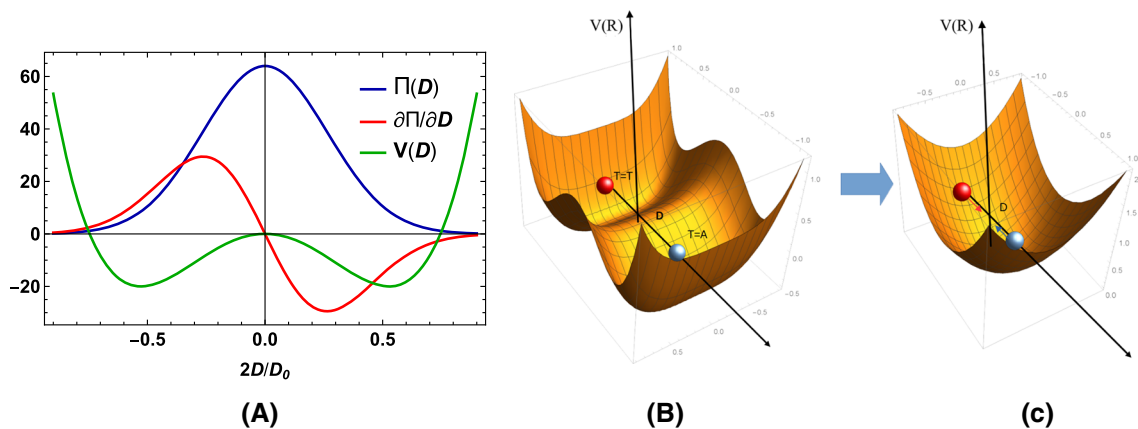


**Fig. 3** (A) The behavior of the polarization function,  $\Pi(D)$ , and its derivative,  $\partial\Pi(D)/(\partial D)$ , in minimums of the double-well potential relative to the common center of mass for the condition  $M_d = M_u = M_n$ . As follows from this representation, the oscillator displacements,  $\Theta_0$  and  $Q_0$ , are proportionally to the derivative function,  $\partial\Pi(D)/(\partial D)$ , and have the opposite signs. The magnitudes of these displacements,  $\Theta_0$  and  $Q_0$ , corresponds to maximal and minimal value of the polarization derivative in these minimum. The transition from double-well potential (B) to single-well potential (C) when UVC field's intensity increases up to a critical value  $I_c$

$$(-\hbar^2 \Delta_\Theta / (2M_d) + M_d \Omega_d^2 \Theta^2 / 2) |n\rangle_d = \hbar \Omega_d (n + 0.5) |n\rangle_d.$$

Here  $\Delta_Q$  and  $\Delta_\Theta$  are the Laplace operators relative to  $\mathbf{Q} = \mathbf{R}_y - \mathbf{R}_{y0}$ , and  $\mathbf{2} = \mathbf{R}_x - \mathbf{R}_{x0}$  displacements of the equilibrium positions of the normal,  $T = A$ , and dimer  $T = T$  states, described in Appendix A.

Now, there could appear a question like: *For which intensity of the applied field, these two states may become mixed?* Looking to the Hamiltonian (A9), we observe that in the harmonic approximation, two oscillation points may coincide when  $Q_i - Q_{0i} - D_0 = \Theta_i - \Theta_{0i}$ . If the nuclei in the both states have same mass, i.e.,  $M_d = M_u = M_n$ , and oscillate in the opposite directions along the  $D_0$ , the projection of the above expression on this direction becomes  $Q - \Theta = D_0 - \Theta_0 + Q_0$ . From the definition of  $\Pi(D)$  in Appendix A follows that this function is even relative to the center of mass as represented in Fig. 3, when the effective mass of the dimer and normal states coincides. In this case,  $-Q_0 = \Theta_0 > 0$ , so we have  $Q - \Theta = D_0 - 2\Theta_0(I)$ . If the UVC field achieves a critical value,  $I_c = M_d \Omega_d^2 D_0 / (2\beta)$ , we may switch to the molecular description of the connected two localized states,  $Q = \Theta$ . In this situation, the Raman-induced scattering process may correlate the dimer and normal DNA states, describing this complex as a new molecular formation for which we can introduce the common generalized coordinate along the direction  $D_0$  as this is represented in Fig. 2.

In order to find the dependence of the number of dimers as a function of the applied intensity of radiation, it is better to switch from the two nuclei coordinates  $Q$  and  $\Theta$  to a common one for both double-well potentials as this is proposed in diatomic molecular vibrations [41]. The position of the dimer along the direction  $D_0$  is  $\Theta$ , and the position of the normal state is  $Q = D + \Theta$ , where  $D$  is the distance between the dimer and normal states. If initially, both states (normal and dimer) of same mass are situated at distance  $D_0$ , the center of mass in the symmetrical vibrations is situated at distance  $D_0/2 = [\Theta M_n + M_n(D + \Theta)] / 2M_n = (2\Theta + D)/2$ , and so follows that  $\Theta = (D_0 - D)/2$ .

The equilibrium position of the state is represented now through the difference between  $D_0$  and the new localized state  $\Theta = (D_0 - D)/2$  (see Fig. 2), so  $D_0/2$  is the position of the center of mass between two thymine/uracil nucleotides in DNA/RNA, respectively, which may be less than 10 Å, and hydrogen bond length in Watson-Crick base pairs is about 1 eV according to [42, 43]. In this case, according to Appendix A, the Hamiltonian of the nuclei (A9) has the aspect of the double-well potential oscillating in anti-phase with the vibration coordinates  $\Theta = (D_0 - D)/2$  and  $Q = (D + D_0)/2$ , see Fig. 3B. If we switch to the center of mass coordinate,  $D_0/2$ , of the quasimolecular system, one obtains the common vibration coordinate,  $-\Theta = Q = D/2$  as is represented in Fig. 3C.

Now it is better to decompose the quasienergetic spectrum of the two sheet potentials relative to the center of the mass  $\Pi(D/2) \approx \Pi(0) + D \partial \Pi(0) / \partial D + (D^2/2) \partial^2 \Pi(0) / (\partial D)^2 + \dots$ . As  $\Pi(D/2)$  is even function, the first derivative in this point is equal to zero,  $\partial \Pi(0) / \partial D = 0$ . The second derivative is negative in the maximum,  $\partial^2 \Pi(0) / (\partial D)^2 < 0$ , so that we have the renormalization of the vibration frequencies of the single-well potential on the intensity action as  $-I \delta_n (D/2)^2$ , where  $\delta_n = |\partial^2 \Pi(0) / (\partial D)^2| / 2$ . In the low quasienergy sheet, the frequency increases after the renormalization, and in the upper one the frequency of the common mode of dimer and normal state decreases, and the Hamiltonian reads

$$\hat{H}^{(n)} = -\frac{\hbar^2}{2\mu} \Delta_D + \frac{[\mu \Omega_n^2 \hat{1} - \hat{\sigma}_z I \delta_n / 2] D^2}{2}$$



$$+ 2\hat{\sigma}_z \Pi(0)I + \delta V(D)\hat{1} + \mathcal{E}_0(D_0)\hat{1}. \quad (9)$$

Here according to Appendix A the displacements of the dimer and normal states depend on the intensity of the applied field with  $\Omega_n = \sqrt{(\Omega_u^2 + \Omega_d^2)/2}$  and  $\mu = M_n/2$  is the reduced mass. Introducing the renormalization frequency for each sheet, i.e.,  $\Omega_{r1} = \sqrt{\Omega_n^2 + I\delta_n/(2\mu)}$  for the lower,  $\Omega_{r2} = \sqrt{\Omega_n^2 - I\delta_n/(2\mu)}$  for the upper one, and by neglecting the higher-order expansion term in the Hamiltonian (9), one obtains two solutions for harmonic oscillators with renormalized frequencies, i.e.,  $\Phi_n^{r_i}(D) \otimes |i\rangle$ ,  $i = 1, 2$ . We observe that this molecular oscillation model works well when  $D_0/2 = \Theta_0(I_c)$ . If the intensity of the applied field is less than the critical value, i.e.,  $I < I_c$ , we can use the perturbation theory switching from one degree of freedom to double-well potential using the small parameter,  $I_c - I$ . Considering that in this case the molecular decoupling takes place, we represent the solution as a superposition described by Exps. (A10), in which one of the terms depends on displacement variables as  $F_n^{r_i}(Q, \Theta) \equiv F_n^{r_i}(Q + |Q_0(I)|, \Theta - \Theta_0(I))$ . For  $I = I_c$ , this function coincides with the solution of the harmonic oscillator,  $\Phi_n^{r_i}(D)$ . In this situation, it is better to represent the argument of the new function through the critical point,  $F_n^{r_i}(Q, \Theta) = \Phi_n^{r_i}(Q + |Q_0(I)|, \Theta - \Theta_0(I)) = F_n^{r_i}(Q + \Theta_0(I_c) - \delta\Theta_0(I), \Theta - \Theta_0(I_c) + \delta\Theta_0(I))$ , where  $\delta\Theta_0(I) = \Theta_0(I_c) - \Theta_0(I)$ . Taking into consideration for the molecular oscillations,  $Q = (D + D_0)/2$  and  $\Theta = (D_0 - D)/2$ , one can observe that in the critical point relative to the position of the center of mass we have  $\delta F(D) = F_n^{r_i}(Q, \Theta)|_{I=I_c} - F_n^{r_i}(Q, \Theta)|_{I_c}$  represented through the common molecular coordinate  $D$  as follows

$$\begin{aligned} \delta F(D) &= 2\partial F_n^{r_i}(Q, \Theta)/\partial D|_{I=I_c} \delta Q_0(I) - 2\partial F_n^{r_i}(Q, \Theta)/\partial D|_{I=I_c} \delta\Theta_0(I) \\ &= -2\partial \Phi_n^{r_i}(D)/\partial D|_{I=I_c} \delta\Theta_0(I); \end{aligned}$$

Here  $F_n^{r_i}(Q, \Theta)|_{I_c} = \Phi_n^{r_i}(D) \otimes |i\rangle$ , and  $\delta\Theta_0(I) = (I_c - I)\hbar/(\mu\Omega_n^2)$  so that the probability of the distorting the quasimolecular complex with the decreasing of the intensity depends on the matrix element  $|\langle \Phi_n^{r_i} | \delta F_n^{r_i} \rangle|^2$  as reads

$$W_{n,n_1} = \frac{4(I_c - I)^2\beta^2}{\mu^2\Omega_n^4} \int dD |\Phi_n^{r_i}(D) \partial \Phi_{n_1}^{r_i}(D) / \partial D|^2.$$

Taking into consideration that the derivative operator  $\partial/\partial D$  may be expressed through annihilation  $\hat{v}$ , and creation  $\hat{v}^\dagger$ , vibron operators, i.e.,  $\partial/\partial D = \sqrt{\mu\Omega_n/(2\hbar)}(\hat{v} - \hat{v}^\dagger)$ . Therefore, one may easily calculate the matrix element,  $\langle \Phi_n^{r_i} | (\hat{v} - \hat{v}^\dagger) | \Phi_{n_1}^{r_i} \rangle = \sqrt{\mu\Omega_n/(2\hbar)}(\sqrt{n_1}\delta_{n,n_1-1} - \sqrt{n}\delta_{n-1,n_1})$ , and so finally the probability becomes

$$W_{n,n_1} = \frac{2(I_c - I)^2\beta^2}{\hbar\mu\Omega_n^3} (\sqrt{n_1}\delta_{n,n_1-1} - \sqrt{n}\delta_{n-1,n_1})^2. \quad (10)$$

As a result, we obtain the quadratic decreasing of dimerization rate with decreasing of the UVC intensity. To carefully study this effect, it is plausible to develop the master equation approach to the induced Raman excitation of the dimerization process described by interaction Hamiltonian (A4) and taking into consideration the thermal bath of the local vibrations of nuclei in normal and dimer bounds. In this situation, the combination between coherent dimer generation in the Raman process and the dephasing process may be described by the phase transition as pointed out by the phenomenological model in Ref. [9]. In the next section, we experimentally estimate this quadratic dependence on the intensity of the inactivation rate of fungal colonies.

### 3 Experimental results: UVC intensity dependence of the decontamination rate

The main part of our equipment described in Refs. [8, 9] consisted of the decontamination core, which is upgraded to a new method by repacking the metamaterial structure with the small quartz balls/fibers, introducing these between the big elements of the metamaterial, as represented in Fig. 4 (A, B, C) and described in the recent Refs. [12, 13]. In this section, we propose to study experimentally the decontamination rate as a function of the intensity of the applied UVC radiation. Therefore, we realized several experiments as represented by the rows in Fig. 5. Each experiment has one more germicidal lamp (18 W of power and wavelength of 254 nm) turn on at the decontamination core, as observed in Fig. 4 (D). In this setup, we use an aluminum cylinder, which reflects the radiation of the UVC lamps around the decontamination core, and so maximally focuses the radiation on the central axis of the core. The role of this cylinder is to protect people from radiation generated by UVC lamps and to make maximum use of the UVC radiation emitted by lamps during the decontamination of fluids flowing through the equipment's core. This core may be filled up by some metamaterials, and we use granulated quartz (transparent to UVC radiation), through which the UVC radiation is propagated inside the infected fluids.

It is known that many pathogens (viruses and bacteria) are more sensible to UVC radiation than eukaryotic cells due to the double protection of DNA by cellular and nucleus membrane of the last. As this, for the proposed experiments we use yeast solutions instead of dangerous contaminated fluids. In fact, the yeast has stronger resistance to UVC radiation in comparison with many viruses or bacteria. The yeast solutions used by us belong to *Saccharomyces cerevisiae* species with the property to form colonies. According to existing investigations, e.g., [47–53], the unicellular organisms have the ability to be arranged in strings of connected budding; the yeast cells are known as pseudohyphae or false hyphae. The cellular life within these populations is a prevalent form of microbial

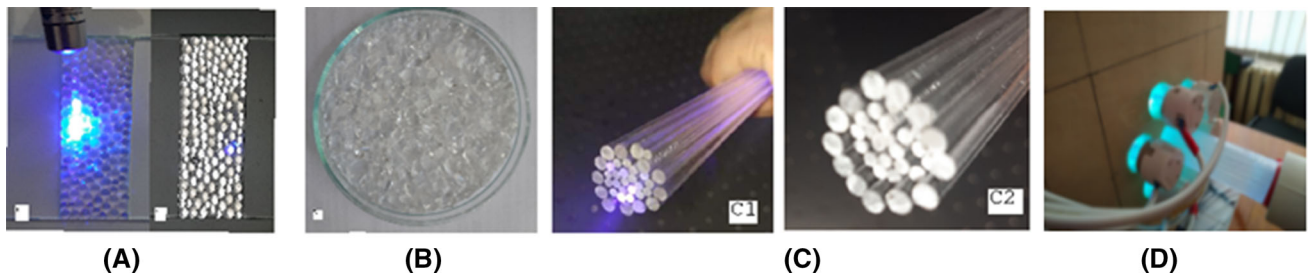


**Fig. 4** The realization of the closed random packing of the small and big spheres (fibers) proposed in our experiments. In (A1) the blue laser is used to shine the sample; (A2) - without blue laser radiation. (B) corresponds to the metamaterials formed from granulated quartz with different dimensions from  $10^{-5}$  mm to 1 mm. (C) represents the packing of two types of optical fibers for the decontamination core of the equipment. As a result, the empty space between the elements of each material, i.e., non-penetrated by UVC radiation, is at the minimal value. In (D), six UVC lamps cover the decontamination core filled up with metamaterials, using the equipment as in (A–C)

existence in natural conditions, so providing the cells with the capabilities to effectively defend against the environmental attacks, as well as efficiently adapt and survive long periods of starvation and other kind of stresses.

As in our previous experiments [12, 13], we prepared samples of yeast solutions by considering the yeast colonies of different size and density (columns a, b, c in Fig. 5) before passing via the decontamination equipment. The experimental design of laboratory tests was constructed to investigate the UVC dose dependence of the inactivation rate for yeast colonies. For each experimental condition, yeast inactivation experiments were conducted randomly and independently to guarantee statistical significance of results. A normal distribution was estimated considering a big number of probe droplets (20–30), but in Fig. 5 only three of these samples are considered. Some statistical dependencies between the geometrical size and number of colonies were established from the experimental observations performed with a microscope with 400x magnification.

The yeast solution samples represented in Fig. 5 evidence an aleatory distribution of colony size in each sample (see columns a, b, c of the first line). Yeast colonies could achieve the dimension of  $1–30\ \mu\text{m}$  in diameter, and we monitored the evolution of the number of yeast colonies as a function of intensity of the UVC irradiation during the decontamination procedure.

So, the metamaterials consisting of quartz fibers or microspheres in optical contact with the yeast samples (Fig. 4) were used. As a result of decontamination procedure, we have obtained the microscopical images shown in the lines of Fig. 5, where the inactivation process of the yeast colonies can be observed. An important part of liquid samples is decontaminated during the time of about 3 min by exposing on the irradiation of six UVC lamps. We emphasize here that this effect is observed in the simple static regime, i.e., when the flow of liquid is stationary between the elements of metamaterial, see also [12, 13]. For the experimental situation represented in Fig. 5, studied in about of 20–30 samples of the decontaminated fluids, one obtains that the mean number of colonies,  $n_0(I)$ , decreases nonlinearly (see Fig. 6A) if turning ON from one to six UVC lamps, so increasing the intensity with the same magnitude in the decontamination core. All six experiments were carried out in the same time interval, equal to 3 min.

For statistical description of the yeast colonies by the ensembles of the experimental samples, we propose to use the Gauss distribution for the number,  $n$ , and diameter,  $d$ , of the yeast colonies defined as

$$W(n, d) = \frac{1}{\sqrt{2\pi}\sigma_n^2} \exp\left[-\frac{(n - n_0)^2}{2\sigma_n^2}\right] \times \frac{1}{\sqrt{2\pi}\sigma_{d_n}^2} \exp\left[-\frac{(d_n - d_{n_0})^2}{2\sigma_{d_n}^2}\right], \quad (11)$$

here  $\sigma_{d_n}$  is the size variance, and  $\sigma_n$  - the number variance of yeast colonies for the same diameters  $d_n$ . To analyze the experimental results, we estimate the average values of the number and size (diameter) of yeast colonies present in samples prepared for decontamination. When no lamp is activated (first row in Fig. 5), we have  $n_0 \approx 50$  and the other parameters are:  $\sigma_n = 2$ ,  $d_{n_0}/d_{sp} = 0.05/n_0$  and  $\sigma_{d_n} = 0.1/d_{sp}$ , where  $d_{sp}$  is visualized diameter of the microscope image, as shown in Fig. 5.

The distribution function of the yeast colonies based on the size parameters depends on the intensity of the UVC applied radiation. The characteristics of the colonies size, like mean number,  $n_0(I)$ , and diameter,  $d_0(I)$ , *de facto* will depend on the number of the irradiating UVC lamps. The consecutive addition of the UVC lamps in the system means that the intensity of the UVC radiation increases proportional to their number,  $I_N \propto N$ , where  $N = 1, 2, \dots, 6$ . In this case, in each experiment, we have the same distribution function as defined in Eq. 11, but with the parameters dependent on the intensity, i.e.,  $n(I)$  and  $d(I)$ . From our estimations, for the case of six UVC lamps one has  $n_0(I_6) \approx 0.08n_0(I = 0)$ , and  $d_0(I_6)/d_{sp} \approx 0.1d_0(I = 0)/d_{sp}$ . Hence, these size parameters, as e.g.,  $n_0$  in Fig. 6, decrease with the increasing of the intensity. If considering there exists a critical intensity,  $I_c$  for which the mean number of yeast colonies and their diameters are zero, i.e.,  $n_0(I_c) = 0$  and  $d_0(I_c) = 0$ , it follows that the increasing of the mean number (diameter) is  $\propto (I_c - I)^2$ , where  $I < I_c$ . In other words

$$n_0(I_N) = \zeta(I_c - I_N)^2 \quad (12)$$

where  $N$  means the number of lamps with  $N < N_c$ , and  $\zeta$  is a constant parameter.

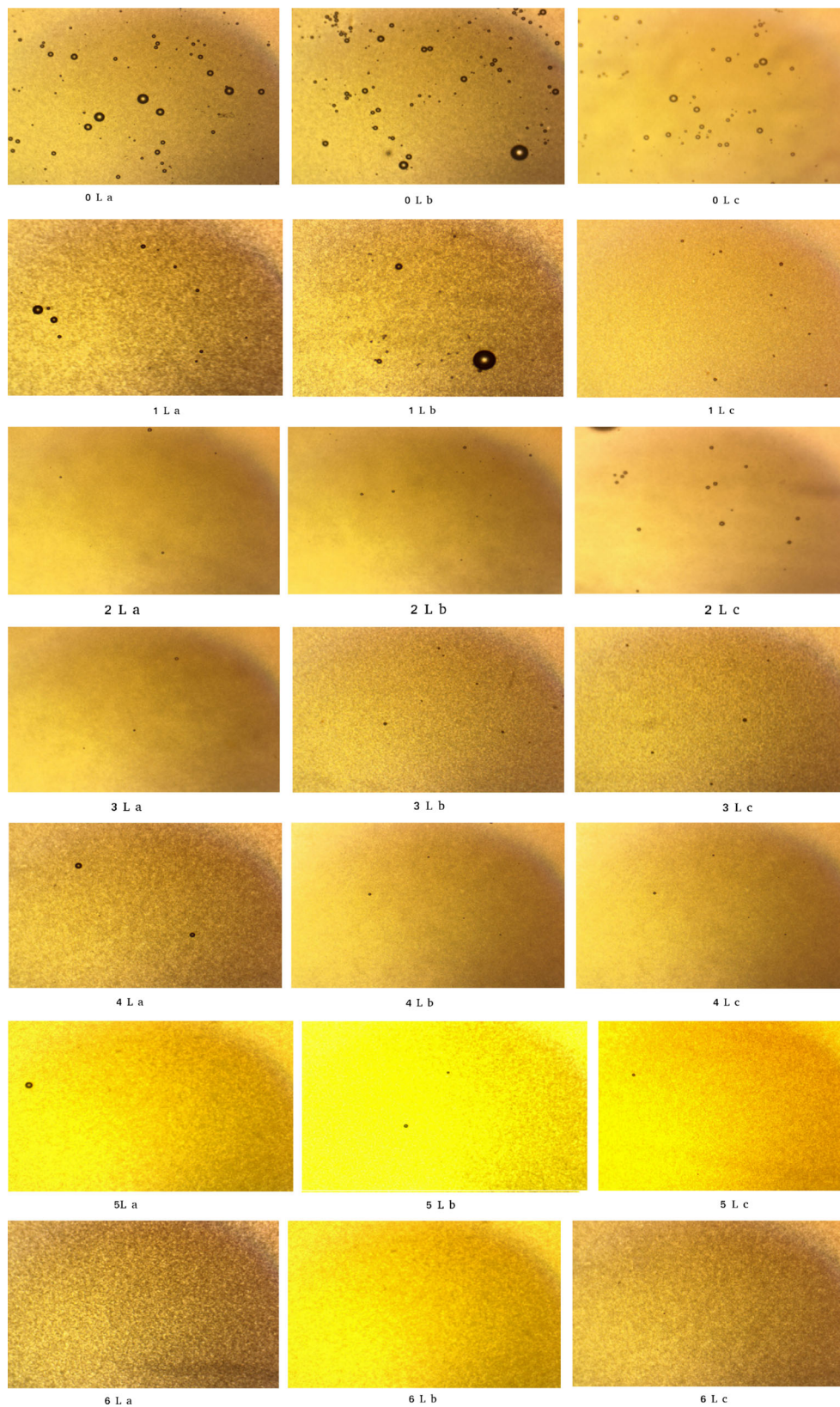


**Fig. 5** Here, each row corresponds consecutively to an experiment with: 0 Lamp, 1 Lamp, 2 Lamps, 3 Lamps, 4 Lamps, 5 Lamps and 6 Lamps, turning on, respectively. In all these experiments, a large number of fluid samples (about 20 – 30) were studied, but one shows only 3 samples of them. It is observed that in such experiments the statistical studies in decontamination rate are necessary in order to establish the inactivation rate (decontamination rate in the case of pathogens)



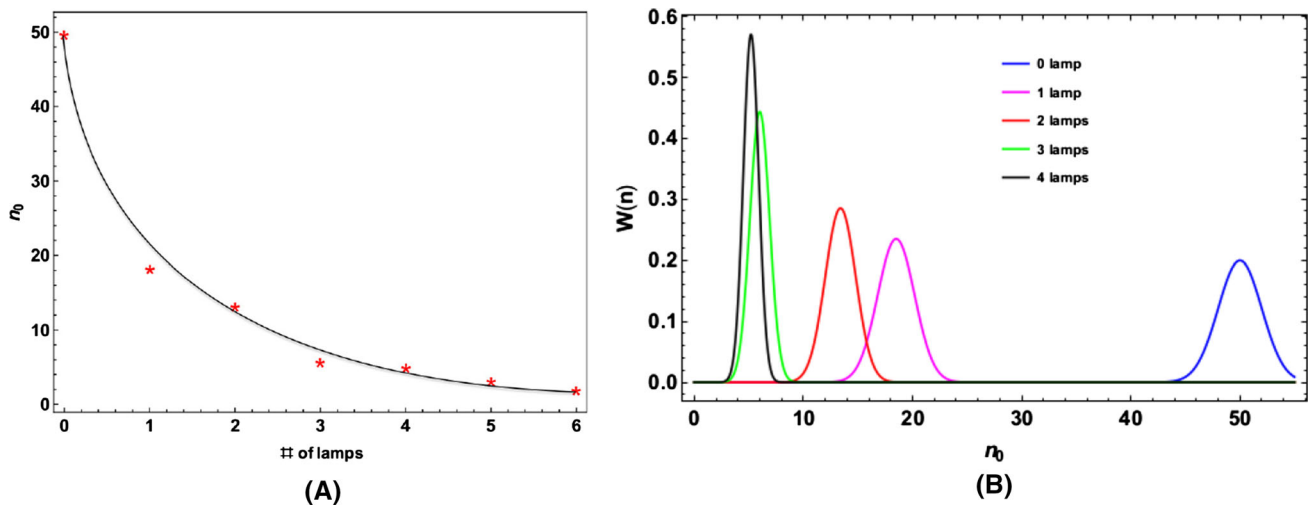


**Fig. 6** (A) The experimental (red stars) and theoretical (blue line) dependencies of the mean number of yeast colonies as a function of the number of UVC lamps turn on. This dependence is equivalent to the intensity one, considering that the radiation intensity obtained from one lamp is about  $5 \text{ mW/cm}^2$  at a distance of 2 cm from the lamp of 18 W. (B) The distribution of yeast colonies as a function of their size (number) for 0 – 4 lamps. It is observed that the small colonies are more affected by UVC radiation and the dispersion decreases with the increasing of the number of lamps

In the experiments described above, for the increasing of penetration depth of UVC radiation into translucent fluids the quartz metamaterials are used. In consequence, this effect optimizes the inactivation rate of contaminator, i.e., the pyrimidine dimerization process of its DNA. These experimental results confirm the good performance of the studied UVC decontamination equipment and serve as a premise that the proposed methodology could be applied with a similar success in case for killing pathogens (bacteria, viruses, fungi, etc.) that may be present in the contaminated fluids.

#### 4 Discussion

As follows from the experimental results, by increasing the intensity of the UVC radiation the inactivation of yeast colonies increases in a strongly nonlinear manner when three radiating lamps are turned on (see Fig. 6A). Afterwards, if consecutively increasing the number of lamps, then a weakly nonlinear law is observed. In our experiments, we used up to six lamps to reach a critical intensity, when almost complete inactivation of the yeast colonies is detected.

Therefore, from these observations, we conclude that by increasing the intensity of the applied radiation in a fixed time interval, the number of yeast colonies decreases nonlinearly up to a given intensity and after, a smooth decreasing prevails. This result confirms the theoretical prediction explained in Sect. 2. Particularly, by taking into consideration the conclusions of the perturbation theory, the intensity dependence of the overlapping of the wave functions in the double-well potential can be applied to this experiment. We may consider the efficiency of the tunneling effect between normal and dimerized DNA states proportional to the shifts defined in the theory as  $\delta Q_0(I) = 2(I_c - I)\alpha/(M\Omega_u^2)$  and  $\delta\Theta_0(I) = 2(I_c - I)\beta/(M\Omega_d^2)$ , so this effect correlates well with the experimental result as observed in Fig. 6A, where a fitting function based on the theoretical result in Eq. 10 is considered. Therefore, one finds a phenomenological correlation between the experimental observations of yeast inactivation dependent on the intensity of irradiation and the theoretical framework explaining the process of dimerization of yeast's DNA by the UVC irradiation. The decontamination parameter of the system becomes proportional to the compression of the double-well potential and the tunneling of the electrons between two stationary states increases as a function of the intensity of the irradiation.

To analyze how the interaction with the UV photons occurs regarding the potential barrier between the normal and dimer states, in the following we make some estimations. For example, in Ref. [56] one finds for haploid yeast cells the mean nuclear volume is  $\sim 3\mu\text{m}^3$  and considering the DNA takes up roughly 0.3% of the nuclear volume, so its dimension can be approximated to about  $0.01\mu\text{m}^3$ . Taking the DNA nuclei as a spherical resonator with the diameter about  $2.15\text{nm}$ , one observes that the UVC radiation can be accumulated in such electromagnetic cavity if the optical density of DNA is larger than this value for the rest of the cell cytoplasm. Finding in [57] that the radiative lifetime may be less than  $1\text{ps}$  for  $\pi\pi^*$  excited states from which we may estimate the dipole transitions,  $P_u$  and  $P_d$  between the excited and two ground states represented in Fig. 1A and, respectively, estimate the displacement of  $Q_0$  and  $\Theta_0$  as explained in Appendix. Indeed, taking into consideration that  $Q_0 = 2I/(M_u\Omega_u^2)$ , where the barrier of oscillators is described by the maximal amplitudes,  $Q_m \sim 5\text{\AA}$  and  $\Theta_m \sim 5\text{\AA}$  of normal and dimer states, we estimate  $M_u\Omega_u^2 Q_m^2/2 \approx M_d\Omega_d^2 \Theta_m^2/2 \sim (0.8 - 1)\text{eV}$ , which corresponds to the intersection of two parabolas in Fig. 2. The shift parameter depends on the work obtained during the action of the generalized force,  $2I\alpha$ , on the nuclei during the displacement,  $Q < Q_m$ , and may be estimated as follows:  $2I\alpha Q \sim 2g_0^2 n P_u P_d Q / (a_g(\hbar\omega_0 - \hbar\omega_u))$ . Here, the mean number of photons can be obtained in the

excitation zone as  $g_0^2 = 2\pi\hbar\omega_0/V$ , where  $V \sim 0.01\mu\text{m}^3$ ,  $\alpha = \partial\Pi(D_0)/\partial R_{y0} \sim \Pi(D_0)/a_g$ ,  $a_g \sim (1-2)\text{\AA}$  is the localization radius of normal state,  $n$  is the mean number of photons. Therefore, if the fluorescence lifetime of the excited state is  $\tau_f \sim \hbar c^3/P_d^2\omega_0^3 < 1\text{ps}$  at wavelength  $330\text{nm}$  (see [57]), we may then calculate not only  $P_d$  and  $P_u$ , but also the Raman detuning from the resonance with the excited state, i.e.,  $\hbar(\omega_0 - \omega_u) = 2\pi\hbar c(1/260\text{nm} - 1/330\text{nm}) \sim 1\text{eV}$ . Finally, the estimation gives the shift energy  $2I\alpha Q_m \sim 1\text{eV}$ , which converges well to  $M_u\Omega_u^2 Q_m^2/2 \sim (0.8 - 1)\text{eV}$ , as mentioned above.

It is well known that the UVC radiation must be used with maximal precaution and security protocols. Nevertheless, to increase the protection of the experimenters from hazardous UVC radiation, a practical recommendation is to close UVC lamps into an aluminum container, moreover that the intensity of the applied UVC radiation in this case can be optimized and then the decontamination process as well. So, multiple reflections of UVC radiation from the aluminum cylinder of decontamination core of the equipment can improve the interaction of pathogens with UVC radiation focused to the center of this cylinder. In the proposed experiments, we have studied this effect as a function of the number of applied UVC lamps inside such a cylinder, through which can be pumped infected fluids (water, air, droplets, aerosols, etc.).

Additional effect to stimulate the decontamination is obtained by introducing quartz fibers/spheres into the translucent contaminated fluids inside the cylinder, so one gets a larger contact surface of the radiation with contaminated fluids. The contact surface consists of the surface of each element multiplied by the number of these. As a result, we end up with a supplementary surface and high distribution of UVC radiation through the whole volume of the contaminated fluids. This method of decontamination may be improved using the short pulses of UVC radiation [54, 55]. Therefore, focusing the radiation inside the decontamination core and using the quartz metamaterials help us to optimize both of the intensity(number) of UVC sources for certain pathogens and exposition time and finally get a feasible critical intensity for almost complete decontamination, particularly, if using low-intensity lamps.

## 5 Conclusions

In summary, in this work we have studied theoretically and experimentally the dependence of the inactivation rate of yeast colonies on the intensity of the applied UVC field. From Fig. 6, it follows that the decontamination process achieves kind of threshold between the strong nonlinear and weak nonlinear dependence on intensity that occurs for about three UVC lamps in our setup. The experimental result is well fitted by the quadratic law obtained from the theoretical model as can be observed in Fig. 6A by the blue line. The critical intensity to inactivate totally the yeast cells is obtained for about six UVC lamps, when these irradiate during 3 minutes.

Finally, we conclude that the results, practical suggestions and methods, discussed throughout this work can be exported to pathogens (viruses and bacteria) to find the correlations between the applied intensity of UVC radiation, exposure time and the type of metamaterials for the dispersion of radiation in translucent fluids (or non-transparent droplets and aerosols). Of course, similar experimental studies can be exported as well to the case of SARS-CoV-2 virus; however, this type of experiment in our laboratory is impossible to carry out due to the absence of the infrastructure and protocols for the manipulation of biological viruses.

**Acknowledgements** This paper was financially supported by the National Agency for Research and Development of Moldova, grant No. 20.80009.5007.01 of State Program (2020 - 2023) and NATO EAP SFPP 984890 project.

**Availability of data and materials** The datasets supporting the conclusions of this article are included within the article sections, figures, and conclusions. The yeast fungal materials and ultraviolet sources were used from the open commercial market for illumination and alimentary preparation.

## Appendix A Elimination of electronic subsystem dressed by scattered UVC field

As we are interested on the structure modification of DNA/RNA by the electronic covalent bonds migrations during the Raman scattering, in the following we consecutively eliminate the virtual states of electron subsystem. We also diagonalize the semiclassical Hamiltonian of atomic and electronic subsystems passing to the system of coordinates rotating with frequency  $(E_{G_u} - E_{G_d})/\hbar$ . In the Born-Markov approximation, the excited state can be represented through the ground states as follows

$$|E(t)\rangle = |E(t)\rangle_0 - \frac{P_u^k g_k}{\hbar(\omega_u - \omega_u^k)} \hat{b}_k^\dagger(t) |G_u(t)\rangle - \frac{P_d^k g_k}{\hbar(\omega_d - \omega_d^k)} \hat{a}_k^\dagger(t) |G_d(t)\rangle \quad (\text{A1})$$

Here  $|E(t)\rangle_0$  is the eigenvector of the free Hamiltonian. After the elimination of the excited state from the interaction Hamiltonian, Eq. 8, one obtains new free and interaction parts of the full Hamiltonian due to the applied field

$$H_0^{eff} = -\hbar\omega_u |G_u\rangle\langle G_u| - \hbar\omega_d |G_d\rangle\langle G_d| + \hbar\omega_u^k \hat{b}_k^\dagger \hat{b}_k + \hbar\omega_d^k \hat{a}_k^\dagger \hat{a}_k$$

$$\begin{aligned}
& - \left\{ \frac{P_u^{k'} g_{k'} P_u^k g_k}{\hbar(\omega_u - \omega_u^{k'})} \hat{b}_{k'}^\dagger(t) \hat{b}_k(t) + H.c. \right\} |G_u(t)\rangle \langle G_u(t)| \\
& - \left\{ \frac{P_d^{k'} g_{k'} P_d^k g_k}{\hbar(\omega_d - \omega_d^{k'})} \hat{a}_{k'}^\dagger(t) \hat{a}_k(t) + H.c. \right\} |G_d(t)\rangle \langle G_d(t)|,
\end{aligned} \quad (A2)$$

$$\begin{aligned}
\hat{H}_{Int}^{eff} = & - \frac{P_u^{k'} g_{k'} P_d^k g_k}{\hbar(\omega_u - \omega_u^{k'})} \hat{b}_{k'}^\dagger(t) \hat{a}_k(t) |G_u(t)\rangle \langle G_d(t)| \\
& - \frac{P_d^{k'} g_{k'} P_u^k g_k}{\hbar(\omega_d - \omega_d^{k'})} \hat{b}_k(t) \hat{a}_{k'}^\dagger(t) |G_d(t)\rangle \langle G_u(t)| + H.c.
\end{aligned} \quad (A3)$$

Now, let us consider in Eqs. (A2, A3) that the applied field is a broadband coherent radiation, then the intensities of the pump field and induced scattered field have the same magnitudes,  $\langle \hat{b}_k^\dagger \hat{b}_k \rangle \approx \langle \hat{a}_k^\dagger \hat{a}_k \rangle$ , and are centered close to the pump frequency  $\omega_p$ . The Raman transitions between the new states are described by the molecular operators,  $\hat{M}^+ = |G_d(t)\rangle \langle G_u(t)|$  and  $\hat{M}^- = |G_u(t)\rangle \langle G_d(t)|$ , which describe the creation and annihilation of dimer state,  $|G_d\rangle$ , during the absorption of higher energy quanta,  $\hat{b}_k$ , and generation of Stokes like one,  $\hat{a}_k^\dagger$ .

Therefore, the electron effective Hamiltonian can be written as follows

$$\hat{H}^{(e)}(\mathbf{R}, t) = \hbar \tilde{\Omega}_0 \hat{M}_z - \Pi I \left\{ \exp[i\Omega_0 t] \hat{M}^- + \exp[-i\Omega_0 t] \hat{M}^+ \right\}, \quad (A4)$$

where  $\hbar \tilde{\Omega}_0 = [\tilde{\mathcal{E}}_d(R_s) - \tilde{\mathcal{E}}_u(R_s)]/2$  is the energy difference between the renormalized energy of dimer and ground states of the nucleobases covalent bound. The operators,  $\hat{M}_z$ ,  $\hat{M}^+$  and  $\hat{M}^-$ , satisfy the commutation relations,  $[\hat{M}^+, \hat{M}^-] = \hat{M}_z$  and  $[\hat{M}_z, \hat{M}^\pm] = \pm \hat{M}^\pm$ , and the second-order susceptibility,  $\Pi(\mathbf{R}) = P_0^2/[\hbar(\omega_d - \omega_0)] + P_0^2/[\hbar(\omega_u - \omega_0)]$  depends on the distance between the dimer,  $T = T$ , and normal,  $T = A$ , localized states,  $\mathbf{D} = \mathbf{R}_x - \mathbf{R}_y$  (see Fig. 2). After the substitution of Eq. (A1) in the interaction Hamiltonian (8), one obtains as well the renormalized energies,  $\mathcal{E}_d(\mathbf{R}) = -\hbar\omega_d - \Pi_0^d I$  and  $\mathcal{E}_u(\mathbf{R}) = -\hbar\omega_u - \Pi_0^u I$ . The energy is measured from the middle point,  $\mathcal{E}_0(\mathbf{R}) = -\hbar(\omega_d + \omega_u)/2$  between the states  $|G_u(t)\rangle$  and  $|G_d(t)\rangle$ . The second-order polarizations,  $\Pi_0^d = 2P_0^2/[\hbar(\omega_d - \omega_0)]$  and  $\Pi_0^u = 2P_0^2/[\hbar(\omega_u - \omega_0)]$  and the intensity of applied UVC field,  $I = \sum_k g_k^2 \langle \hat{b}_k^\dagger \hat{b}_k \rangle$ , results from the Hamiltonian part (A2) by replacing the coefficients and field frequencies by their average values,  $P_u^k \approx P_d^k \approx P_0$ ;  $\omega_u^k \approx \omega_d^k \approx \omega_0$ . Similar expressions were used in the interaction part of the Hamiltonian (A3) as well. Here it was considered that the scattered and absorbed photons from the bimodal field of UVC radiation act as Raman excitation of pyrimidine dimers with the induced frequency  $\omega_d^k - \omega_u^{k'} \approx \Omega_0$ , where  $\Omega_0 = \omega_d - \omega_u$  is the excitation frequency of dimer without renormalization. The intensity  $I = E_0(\omega_u)E_0(\omega_d)$  may be considered of the same magnitude as the intensity  $I$  for the broadband coherent radiation.

In the following, let's study in detail the nuclear subsystem, where we consider that in these two types of covalent bonds participate some conglomerate of atoms, which may form pyrimidine or other kind of dimer. According to the BO approximation, we can return to the coordinates of the nuclear subsystem, considering that in the initial system the nuclei may have two wells of oscillations: one corresponds to the normal DNA/RNA state and another to dimer localization. Therefore, the Hamiltonian of the nuclei subsystem reads

$$\hat{H}^{(n)}(\mathbf{R}) = \sum_j \frac{\hat{p}_j^2}{2M_j} + \hat{\mathcal{E}}_0(\mathbf{R}). \quad (A5)$$

The localized normal,  $|G_u\rangle$ , and dimer,  $|G_d\rangle$ , states must be found from the minimum of the position of this two-level system characterized by the bond energy,  $\mathcal{E}_0(\mathbf{R})$ , the minimum of which according to the BO approach in the estimation of such energy can be considered  $\mathcal{E}_0(\mathbf{R}_0)$ , where according to Fig. 2 the potential sheet contains two minima  $\mathbf{R}_0 \equiv \{\mathbf{R}_{y0}, \mathbf{R}_{x0}\}$ . According to this representation, we may introduce the new generalized oscillation coordinates relative to the minimal energy of the normal and dimer states of the DNA section,  $Q = R_y - R_{y0}$  and  $\Theta = R_x - R_{x0}$ , and estimate the oscillation energy relative to these minima situated at distance  $D_0 = |\mathbf{R}_{y0} - \mathbf{R}_{x0}|$ . In the literature, it is found that  $|\mathbf{R}_{y0}| \sim 10 \text{ \AA}$ , representing the position of  $T = A$  bond position relative to one of each strand and  $|\mathbf{R}_{x0}|$  is less than the distance between two consecutive bases, i.e.,  $\sim 3.4 \text{ \AA}$  (see Fig. 1B). The distance,  $D_0$ , according to the literature [42] may be less than  $10 \text{ \AA}$ . In Eq. (A5), one can introduce the potential function,  $\hat{V}(\mathbf{R}_s - \mathbf{R}_{s0}) = \hat{\mathcal{E}}_0(\mathbf{R}) - \hat{\mathcal{E}}_0(\mathbf{R}_0)$ ,  $s = \{x, y\}$ , which is finally decomposed in the Taylor series as  $\hat{V}(\mathbf{R}_s - \mathbf{R}_{s0}) = [\hat{Q}_j^2 \partial^2 V(0)/(\partial Q_j^2) + \hat{\Theta}_j^2 \partial^2 V(0)/(\partial \Theta_j^2)]/2 + \delta \hat{V}$ . Here, the first-order terms were neglected, considering that in the absence of the external field one uses the property of the symmetry,  $V(-x) = V(x)$ , and the higher-order terms are included in  $\delta \hat{V}(Q, \Theta)$ , particularly studied in Ref. [10]. As a result of these transformations, one gets the Hamiltonian for the nuclei in a new form

$$\hat{H}^{(n)}(\mathbf{R}) = \frac{\hat{p}_u^2}{2M_u} + \frac{M_u \Omega_u^2 \hat{Q}^2}{2} + \frac{\hat{p}_d^2}{2M_d} + \frac{M_d \Omega_d^2 \hat{\Theta}^2}{2} + \delta \hat{V}(Q, \Theta) + \hat{\mathcal{E}}_0(\mathbf{R}_0), \quad (A6)$$

where  $M_u \Omega_u^2 = \partial^2 V(0)/(\partial Q^2)$  and  $M_d \Omega_d^2 = \partial^2 V(0)/(\partial \Theta^2)$ , here  $M_u$  ( $M_d$ ) and  $\Omega_u$  ( $\Omega_d$ ) are the nucleus effective mass and oscillation frequency, respectively, in the normal (dimer) localization. The influence of the applied UVC field on the vibrational nuclear excitation permits us to describe the wave function of the nuclei as a spinor state

$$-i\hbar \frac{d}{dt} |\chi(\mathbf{R})\rangle = \left( \hat{H}^{(n)}(\mathbf{R}) + \hat{H}^{(e)}(\mathbf{R}, t) \right) |\chi(\mathbf{R})\rangle, \quad (\text{A7})$$

where the 'ket' vector,  $|\chi(\mathbf{R})\rangle$ , is a Hermitian conjugate of the 'bra' one, which is defined as a line vector with two components of the electronic states, i.e.,  $\langle \chi(\mathbf{R})| = (\chi_1(\mathbf{R}), \chi_2(\mathbf{R}))$ .

In Eq. (A7),  $H^{(e)}$  is the electron effective Hamiltonian (A4), which can be reduced to the stationary states of the quasienergies in the coordinate system rotating with the frequency  $\Omega_0$  by splitting two states corresponding to dimer and normal DNA/RNA, i.e.,  $H^{(e)} = \hbar \tilde{\Omega} U_z$ . Here, the dynamical Stark splitting frequency is defined as  $\tilde{\Omega} = \sqrt{(\tilde{\Omega}_0 - \Omega_0)^2 + 4(\Pi I/\hbar)^2}$ . Therefore, one observes that the external field improves the 'tunneling' from normal state,  $|G_u\rangle$  to the pyrimidine dimer one,  $|G_d\rangle$ , due to the fact that the Rabi frequency increases proportionally to the intensity of the applied UVC field. This effect will be notable if considering that the energies  $\hbar\omega_u$  and  $\hbar\omega_d$  are small as compared to the normalized energies, so that the second-order polarizations can be approximated as follows:  $\Pi_0^d = 2P_0^2/[\tilde{\mathcal{E}}_0 + \hbar\Omega_0/2 - \hbar\omega_0] \approx 2P_0^2/[\tilde{\mathcal{E}}_0 - \hbar\omega_0] - \hbar\Omega_0/(\tilde{\mathcal{E}}_0 - \hbar\omega_0)^2$  and  $\Pi_0^u = 2P_0^2/[\mathcal{E}_0(\mathbf{R}) - \hbar\Omega_0/2 - \hbar\omega_0] \approx 2P_0^2/[\mathcal{E}_0(\mathbf{R}) - \hbar\omega_0] + \hbar\Omega_0/(\mathcal{E}_0(\mathbf{R}) - \hbar\omega_0)^2$ . In this situation, the splitting energy represented by the first term of the Hamiltonian (A4) is proportional to the Stark shift,  $\hbar\Omega_0 P_0^2 I/(\mathcal{E}_0(\mathbf{R}) - \hbar\omega_0)^2$ . As the polarization matrix element,  $P_0(\mathbf{D})$ , describes the transition between the shifted normal,  $T = A$  and dimer,  $T = T$ , states and excited one, the last expression points out that the increase of the intensity,  $I$ , of the applied radiation, will amplify the splitting energy between normal and dimer states, so shifting them. The last dependence demonstrates the modification of the potential barrier in the adiabatic process under the action of UVC radiation, so improving electron tunneling from the normal state to a dimer one.

Considering that the splitting energy related to the Raman transition is larger than the local energy of each normal or dimer oscillator, i.e.,  $\Omega_0 \gg \{\Omega_u, \Omega_d\}$ , so we can go to the coordinate system rotating with  $\Omega_0$  the Hamiltonian in Eq. (A7), i.e.,  $\exp[i\Omega_0 \hat{M}_z t](\hat{H}^{(n)}(\mathbf{R}) + \hat{H}^{(e)}(\mathbf{R}, t)) \exp[-i\Omega_0 \hat{M}_z t]$ . In this situation, the time-independent electron interaction part of the Hamiltonian,  $-\Pi I_0(\hat{M}^- + \hat{M}^+)$ , is obtained applying the BO approximation, which concludes that during the rotation with rapid frequency,  $\Omega_0$ , the nuclear part of the Hamiltonian,  $\hat{H}^{(n)}(\mathbf{R})$ , is not affected. For simplicity, we may consider that the frequencies and nuclear mass of both oscillators have the same magnitudes, i.e., using the approximation  $\Omega_u \approx \Omega_d$  and  $M_u \approx M_d$  in the representation of the stationary Schrödinger equation (A7), which reduces to

$$0 = \begin{bmatrix} \hat{H}_0(\mathbf{R}) + \hbar(\tilde{\Omega}_0 - \Omega_0)/2 - \mathcal{E} & \Pi I \\ \Pi I & \hat{H}_0(\mathbf{R}) - \hbar(\tilde{\Omega}_0 - \Omega_0)/2 - \mathcal{E} \end{bmatrix} \begin{bmatrix} \chi_1(\mathbf{R}) \\ \chi_2(\mathbf{R}) \end{bmatrix}$$

and from which follows the energy of the two splitting states

$$E_{1,2}(I) = \frac{P_u^2}{2M_u} + \frac{M_u \Omega_u^2 Q^2}{2} + \frac{P_d^2}{2M_d} + \frac{M_d \Omega_d^2 \Theta^2}{2} + \mathcal{E}_0(R_0) \mp \frac{\hbar}{2} \sqrt{(\tilde{\Omega}_0 - \Omega_0)^2 + 4(\Pi(R)I/\hbar)^2}. \quad (\text{A8})$$

For simplicity, we consider that  $M_n = M_u = M_d$ , and  $\Omega_u = \Omega_d$ . As a result, under the approach  $\tilde{\Omega}_0 - \Omega_0 \approx \Omega_0 P_0^2 I/(\mathcal{E}_0 - \hbar\omega_0)^2$ , and for small detuning,  $\tilde{\Omega}_0 - \Omega_0 \ll 2\Pi I_0$ , the energy of the double-well oscillator is reduced to the expression,  $E_{1,2}(I) \approx H_0(\mathbf{R}) \mp \Pi(\mathbf{Q})I$ . Here, it was considered that the transition energy satisfies the condition:  $\hbar\Omega_0 < (\tilde{\mathcal{E}}_0 - \hbar\omega_0)$ . In this situation, the susceptibility depends on the oscillator coordinate,  $\Pi(\mathbf{Q})$  and can be decomposed in Taylor series,  $\Pi(\mathbf{Q}, \mathbf{2}) \approx \Pi(\mathbf{R}_{y0}, \mathbf{R}_{x0}) + (\mathbf{Q}, \partial \Pi(\mathbf{R}_{x0}, \mathbf{R}_{y0})/\partial \mathbf{R}_{y0}) + (\mathbf{2}, \partial \Pi(\mathbf{R}_{x0}, \mathbf{R}_{y0})/\partial \mathbf{R}_{x0}) + \dots$ . Taking into consideration that in our simplified model, the polarization  $\Pi(\mathbf{R}_{y0}, \mathbf{R}_{x0}) = \Pi(\mathbf{D}_0)$  contains the oscillatory modes in two quantum wells with normal modes,  $\mathbf{Q}$  for normal state and  $\mathbf{2}$  for DNA or RNA dimer, and separated by the distance  $\mathbf{D}_0 = \mathbf{R}_{y0} - \mathbf{R}_{x0}$ , so one observes that  $\partial \Pi(\mathbf{D}_0)/\partial \mathbf{R}_{y0} = -\partial \Pi(\mathbf{D}_0)/\partial \mathbf{R}_{x0}$ , for the same mass in the dimer and normal states. In this situation, we obtain that the external field shifts the oscillation point of each covalent sheet state quasienergies,  $V_1 = [M_u \Omega_u^2 Q^2 + M_d \Omega_d^2 \Theta^2]/2 - 2I\alpha_i Q_i - 2I\beta_i \Theta_i - 2\Pi(\mathbf{D}_0)I + \mathcal{E}_0(\mathbf{Q})$ ,  $V_2 = [M_u \Omega_u^2 Q^2 + M_d \Omega_d^2 \Theta^2]/2 + 2I\alpha_i Q_i + 2I\beta_i \Theta_i + 2\Pi(\mathbf{D}_0)I + \mathcal{E}_0(\mathbf{Q})$ , here  $i = \{x, y, z\}$ . The parameters  $\alpha_i = \partial \Pi(\mathbf{D}_0)/\partial R_{y0,i}$  and  $\beta_i = \partial \Pi(\mathbf{D}_0)/\partial R_{x0,i}$  are the gradient components. Now, transforming the energy of the potential well to a quadratic form, one gets

$$\begin{aligned} \hat{H} &= \frac{\hat{P}_u^2}{2M_u} + \frac{\hat{P}_d^2}{2M_d} + M_u \Omega_u^2 (Q\hat{1} + Q_0\hat{\sigma}_z)^2/2 - M_d \Omega_d^2 (\Theta\hat{1} + \Theta_0\hat{\sigma}_z)^2/2 \\ &= -2I^2 \left( \frac{\alpha^2}{M_u \Omega_u^2} + \frac{\beta^2}{M_d \Omega_d^2} \right) \hat{1} + 2I\Pi(\mathbf{D}_0)\hat{\sigma}_z + \delta V(Q, \Theta)\hat{1} + \mathcal{E}_0(\mathbf{R}_0)\hat{1}, \end{aligned} \quad (\text{A9})$$

where  $Q_0 = 2I/(M_u \Omega_u^2)$ ,  $\Theta_0 = 2I\hbar/(M_d \Omega_d^2)$ ;  $\hat{\sigma}_z = |2\rangle\langle 2| - |1\rangle\langle 1|$  and  $\hat{1} = |2\rangle\langle 2| + |1\rangle\langle 1|$  are the common sigma- $z$  Pauli and identity matrices, respectively, taking into consideration the two sheets numbered by "1" the lower, and by "2" the upper one.



Neglecting the higher-order potential decomposition, i.e.,  $\delta\hat{V} = 0$ , we obtain the solutions for the shifted oscillators, for the lower and upper sheets, respectively:

$$\begin{aligned} |\chi_1(R)\rangle &\sim \Phi_n^u(Q - Q_0)\Phi_n^d(\Theta - \Theta_0) \otimes |1\rangle, \\ |\chi_2(R)\rangle &\sim \Phi_n^u(Q + Q_0)\Phi_n^d(\Theta + \Theta_0) \otimes |2\rangle. \end{aligned} \quad (\text{A10})$$

Here  $\Phi_n(Z_i - Z_{i0})$  is the eigenfunction of the traditional harmonic oscillator shifted by the field,  $Z_{i0}$  relative to the equilibrium position in the absence of radiation,  $Z_i \equiv \{Q_i, \Theta_i\}$ ,  $i = \{x, y, z\}$ . Considering that initially the system is prepared in a normal state,  $|\chi_1(\mathbf{R})\rangle = |1\rangle$ , the transition from normal to dimer states is described by the operator  $\hat{\sigma}^+ = |2\rangle\langle 1|$ .

In conclusion, we observe that the intensity of the applied UVC field shifts the position of nuclei during the scattering process stimulating the tunneling of an electron from one potential well to another. This effect corresponds to coherent excitation of the nuclei vibrations relative to the stationary localized states, and so resulting in the transformation and modification of DNA under the UVC radiation.

## References

- B. Ma, P.M. Gundy, C.P. Gerba, M.D. Sobsey, UV Inactivation of SARS-CoV-2 across the UVC spectrum: KrCl\* excimer, mercury-vapor, and LED sources. *Appl. Environ. Microbiol.* **87**, e01532-21 (2021). <https://doi.org/10.1128/AEM.01532-21>
- M. Biasin, A. Bianco, G. Pareschi et al., UV-C irradiation is highly effective in inactivating SARS-CoV-2 replication. *Sci. Rep.* **11**, 6260 (2021). <https://doi.org/10.1038/s41598-021-85425-w>
- F. Chiappa, B. Frascella, G.P. Vigezzi, M. Moro, L. Diamanti, L. Gentile, P. Lago, N. Clementi, C. Signorelli, N. Mancini et al., The efficacy of ultraviolet light-emitting technology against coronaviruses: A systematic review. *J. Hosp. Infect.* **114**, 63 (2021). <https://doi.org/10.1016/j.jhin.2021.05.005>
- H. Shimoda, J. Matsuda, T. Iwasaki, D. Hayasaka, Efficacy of 265-nm ultraviolet light in inactivating infectious SARS-CoV-2. *J. Photochem. Photobiol.* **7**, 100050 (2021). <https://doi.org/10.1016/j.jpap.2021.100050>
- M. Heßling, K. Hones, P. Vatter, C. Lingenfelder, Ultraviolet irradiation doses for coronavirus inactivation - review and analysis of coronavirus photoinactivation studies, *GMS Hyg. Infect. Control.* 15:08 (2020). DOI 10.3205/dgkh000343
- M. Buonanno, D. Welch, I. Shuryak, J. David, Far-UVC light (222 nm) efficiently and safely inactivates airborne human coronaviruses. *Sci. Rep.* **10**, 10285 (2020). <https://doi.org/10.1038/s41598-020-67211-2>
- M. Peng, A.J. Brown, S. Esaki, S. Lockwood, G.M.K. Poon, M.J. Smerdon, S.A. Roberts, J.J. Wyrick, ETS transcription factors induce a unique UV damage signature that drives recurrent mutagenesis in melanoma. *Nature Commun.* **9**, 2626 (2018). <https://doi.org/10.1038/s41467-018-05064-0>
- N.A. Enaki, A. Profir, N. Ciobanu, S. Bazgan, A. Nisteanu, M. Turcan, E. Starodub, T. Pislari, C. Ristoscu, M. Badiceanu, I.N. Mihailescu, Optical metamaterials for decontamination of translucent liquids and gases. *J. Phys. D* **51**, 385101 (2018). <https://doi.org/10.1088/1361-6463/aad705>
- N.A. Enaki, S. Bazgan, N. Ciobanu, M. Turcan, T. Pislari, C. Ristoscu, A. Vaseaseasta, I.N. Mihailescu, Improvement in ultraviolet based decontamination rate using metamaterials. *Appl. Surface Sci.* **417**, 40 (2017). <https://doi.org/10.1016/j.apsusc.2017.01.133>
- N. Enaki, S. Bizgan, A. Nisteanu, V. Tonu, M. Turcan, T. Pislari, E. Starodub, A. Profir, G.-F. Popescu-Pelin, M. Badiceanu, C.-G. Ristoscu and I. N. Mihailescu, Efficient microbial decontamination of translucent liquids and gases using optical metamaterials, in the book "Advanced Surface Engineering Research". (IntechOpen Book Series, 2018). <https://doi.org/10.5772/intechopen.80639>
- N.A. Enaki, T. Turcan, S. Bazgan, E. Starodub, T. Pislari, A. Nisteanu, C. Ristoscu, I.N. Mihailescu, Composite metamaterials for biological decontamination of fluids, in *IFMBE Proceedings*. (Springer, London, 2020), pp.10–16
- N.A. Enaki, E. Starodub, T. Pislari, M. Turcan, S. Bazgan, Close packing of elements of transparent metamaterials in UVC diapason and its influence on the decontamination efficiency. *J. Immunol. Infect. Dis.* **8**, 104 (2021)
- N.A. Enaki, E. Starodub, T. Pislari, M. Turcan, S. Bazgan, Increasing of decontamination rate of infected fluid by rotation channels under the dispersion of ultraviolet C radiation by composite metamaterial. *Phys. Sci. Biophys. J.* **5**, 000188 (2021)
- H.H. Lans, J.H.J. Hoeijmakers, W. Vermeulen, J.A. Marteijn, The DNA damage response to transcription stress. *Nat. Rev. Mol. Cell Biol.* **20**, 766 (2019). <https://doi.org/10.1038/s41580-019-0169-4>
- J.A. Marteijn, H. Lans, W. Vermeulen, J.H.J. Hoeijmakers, Understanding nucleotide excision repair and its roles in cancer and ageing. *Nat. Rev. Mol. Cell Biol.* **15**, 465 (2014). <https://doi.org/10.1038/nrm3822>
- M. Pinak, Enzymatic recognition of radiation-produced oxidative DNA lesion: Molecular dynamics approach. *Modern Methods Theoret. Phys. Chem. Biopol.* **10**, 191 (2006). <https://doi.org/10.1016/B978-044452220-7/50074-5>
- V.V. Ogryzko, A quantum-theoretical approach to the phenomenon of directed mutations in bacteria (hypothesis). *Biosystems* **43**, 83 (1997). [https://doi.org/10.1016/S0303-2647\(97\)00030-0](https://doi.org/10.1016/S0303-2647(97)00030-0)
- J. McFadden, J.S. Al-Khalili, A quantum mechanical model of adaptive mutation. *Biosystems* **50**, 203 (1999). [https://doi.org/10.1016/S0303-2647\(99\)00004-0](https://doi.org/10.1016/S0303-2647(99)00004-0)
- G.S. Engel, T.R. Calhoun, E.L. Read et al., Evidence for wavelike energy transfer through quantum coherence in photosynthetic systems. *Nature* **446**, 782 (2007). <https://doi.org/10.1038/nature05678>
- G. Panitchayangkoon, D. Hayes, K.A. Fransted et al., Long-lived quantum coherence in photosynthetic complexes at physiological temperature. *Proc. Natl. Acad. Sci. USA* **107**, 12766 (2010). <https://doi.org/10.1073/pnas.1005484107>
- E. Collini, C.Y. Wong, K.E. Wilk et al., Coherently wired light-harvesting in photosynthetic marine algae at ambient temperature. *Nature* **463**, 644 (2010)
- Quantum Aspects of Life*, edited by D. Abbott, P.C.W. Davies, A.K. Pati. (2008) Imperial College Press: London
- Quantum Effects, in *Biology*, edited by M. Mohseni, Y. Omar, G.S. Engel, M.B., *Plenio* (Cambridge University Press, Cambridge, 2014)
- L. Slocombe, J.S. Al-Khalili, M. Sacchi, Quantum and classical effects in DNA point mutations: Watson-Crick tautomerism in AT and GC base pairs. *Phys. Chem. Chem. Phys.* **23**, 4141 (2021). <https://doi.org/10.1039/D0CP05781A>
- Y. Kim, F. Bertagna, E.M. D'Souza et al., Quantum Biology: an update and perspective. *Quantum Rep.* **3**, 80 (2021). <https://doi.org/10.3390/quantum3010006>
- A.D. Godbeer, J.S. Al-Khalili, P.D. Stevenson, Modelling proton tunnelling in the adenine-thymine base pair. *Phys. Chem. Chem. Phys.* **17**, 13034 (2015). <https://doi.org/10.1039/C5CP00472A>

27. J.C. Brookes, Quantum effects in biology: golden rule in enzymes, olfaction, photosynthesis and magnetodetection. *Proc. R. Soc. A* **473**, 20160822 (2017). <https://doi.org/10.1098/rspa.2016.0822>
28. A.V. Melkikh, A. Khrennikov, Nontrivial quantum and quantum-like effects in biosystems: Unsolved questions and paradoxes. *Progr. in Biophys and Molec. Biology* **119**, 137 (2015). <https://doi.org/10.1016/j.pbiomolbio.2015.07.001>
29. E. Brunk, U. Rothlisberger, Mixed quantum mechanical/molecular mechanical molecular dynamics simulations of biological systems in ground and electronically excited states. *Chem. Rev.* **115**, 6217 (2015). <https://doi.org/10.1021/cr500628b>
30. D. Santiago-Alarcon, H. Tapia-McClung, S. Lerma-Hernandez, S.E. Venegas-Andraca, Quantum aspects of evolution: a contribution towards evolutionary explorations of genotype networks via quantum walks. *J. R. Soc. Interface* **17**, 20200567 (2020)
31. M. Born, J. R. Oppenheimer., Zur Quantentheorie der Molekeln [On the Quantum Theory of Molecules]. *Annalen der Physik (in German)*. **389**(20), 457–461 (1927)
32. R. Loudon, *The Quantum theory of light* (In Press, Oxford, 2000), p.448
33. A. Kuzminov, Pyrimidine dimers, Brenner's Encyclopedia of. *Genetics* **5**, 538 (2013). <https://doi.org/10.1016/B978-0-12-374984-0.01244-4>
34. W.J. Schreier, W.J. Schrader, F.O. Koller, P. Gilch, C.E. Crespo-Hernandez, V.N. Swaminathan, T. Carell, W. Zinth, B. Kohler, Thymine dimerization in DNA is an ultrafast photoreaction. *Science* **315**, 625 (2007). <https://doi.org/10.1126/science.1135428>
35. R.P. Rastogi, A. Richa, M.B. Kumar, R.P. Sinha. Tyagi, Molecular mechanisms of ultraviolet radiation-induced DNA damage and repair. *J. Nucleic Acids* **2010**, 592980 (2010)
36. W. Kowalski, *Ultraviolet germicidal irradiation handbook. UVGI for Air and surface disinfection*. (Springer, 2009), p.17-50. <http://www.springer.com/978-3-642-01998-2>
37. F.L. Pilar, *Element. Quant. Chem.* (McGraw-Hill, New York, 1968)
38. V.K. Jaiswal, J. Segarra-Marti, M. Marazzi, E. Zvereva, X. Assfeld, A. Monari, M. Garavelli, I. Rivalta, First-principles characterization of the singlet excited state manifold in DNA/RNA nucleobases. *Phys. Chem. Chem. Phys.* **22**, 15496 (2020). <https://doi.org/10.1039/D0CP01823F>
39. C. Marian, D. Nolting, R. Weinkauff, The electronic spectrum of protonated adenine: Theory and experiment. *Phys. Chem. Chem. Phys.* **7**, 3306 (2005). <https://doi.org/10.1039/B507422C>
40. C.R. Martinez, B.L. Iverson, Rethinking the term 'pi-stacking'. *Chem. Sci.* **3**, 2191 (2012). <https://doi.org/10.1039/C2SC20045G>
41. E. Bright Wilson, J. C. Decius, P. C. Cross, *Molecular Vibrations*. (Dover Publications, 2012)
42. J.L. Huret et al., Atlas of genetics and cytogenetics in oncology and haematology in 2013. *Nucleic Acids Res.* **41**, 19–24 (2013)
43. C.F. Guerra, F.M. Bickelhaupt, J.G. Snijders, E.J. Baerends, Hydrogen Bonding in DNA Base Pairs: Reconciliation of Theory and Experiment. *J. Am. Chem. Soc.* **122**(17), 4117 (2000). <https://doi.org/10.1021/ja993262d>
44. H.G. Duan, V. I. Prokhorenko, R. J. Cogdell, K. Ashraf, A. L. Stevens, M. Thorwart, R. J. Dwayne Miller, Nature does not rely on long-lived electronic quantum coherence for photosynthetic energy transfer, *Proceedings of the National Academy of Sciences*, **114**, 8493 (2017). <https://doi.org/10.1073/pnas.1702261114>
45. E. Z. Harush, Y. Dubi, Do photosynthetic complexes use quantum coherence to increase their efficiency? Probably not, *Sci. Adv.* **7**, eabc4631 (2021). <https://doi.org/10.1126/sciadv.abc4631>
46. N.R. Baker, Chlorophyll fluorescence: a probe of photosynthesis in vivo. *Annual Rev. Plant Biol.* **59**, 89 (2008). <https://doi.org/10.1146/annurev.arplant.59.032607.092759>
47. E. Yong, Yeast suggests speedy start for multicellular life. *Nature* (2012). <https://doi.org/10.1038/nature.2012.9810>
48. W.C. Ratcliff, R.F. Denison, M. Borrello, M. Travisano, Experimental evolution of multicellularity. *Proc. Natl. Acad. Sci. USA* **109**, 1595 (2012). <https://doi.org/10.1073/pnas.1115323109>
49. M.E. Boraas, D.B. Seale, J.E. Boxhorn, Phagotrophy by a flagellate selects for colonial prey: A possible origin of multicellularity. *Evol. Ecology* **12**, 153 (1998). <https://doi.org/10.1023/A:1006527528063>
50. J. H. Koschwanez, K. R. Foster, A. W. Murray. (2011). Sucrose utilization in budding yeast as a model for the origin of undifferentiated multicellularity. *PLoS Biology*. **9**(8): 10.1371
51. *Biodiversity and ecophysiology of yeasts*, edited by G. Peter and C. Rosa. Springer: London. (2006)
52. K. Walkeellipser, H. Skelton, K. Smith, Cutaneous lesions showing giant yeast forms of *Blastomyces dermatitidis*. *J. Cutaneous Pathology* **29**, 616 (2002). <https://doi.org/10.1034/j.1600-0560.2002.291009.x>
53. J.L. Legras, D. Merdinoglu, J.M. Cornuet, F. Karst, Bread, beer and wine: *Saccharomyces cerevisiae* diversity reflects human history. *Molecular Ecology* **16**(10), 2091–102 (2007). <https://doi.org/10.1111/j.1365-294x.2007.03266.x>
54. R. Mandal, X. Mohammadi, A. Wiktor, A. Singh, A.P. Singh, Applications of pulsed light decontamination technology in food processing: An overview. *Appl. Sci.* **10**, 3606 (2020). <https://doi.org/10.3390/app10103606>
55. J. Jean, M.I. Rodriguez-Lopez, E. Jubinville, E. Nunez-Delgado, V.M. Gomez-Lopez, Potential of pulsed light technology for control of SARS-CoV-2 in hospital environments. *J. Photochem. Photobiol. B: Biol.* **215**, 112106 (2021). <https://doi.org/10.1016/j.jphotobiol.2020.112106>
56. R. Millo, B. Phillips, *Cell Biology by the numbers* (Garland Science, New York, 2015)
57. C.E. Crespo-Hernandez, B. Cohen, P.M. Hare, B. Kohler, Ultrafast excited-state dynamics in Nucleic Acids. *Chem. Rev.* **104**(4), 1977 (2004). <https://doi.org/10.1021/cr0206770>

Springer Nature or its licensor holds exclusive rights to this article under a publishing agreement with the author(s) or other rightsholder(s); author self-archiving of the accepted manuscript version of this article is solely governed by the terms of such publishing agreement and applicable law.